Progress In Electromagnetics Research, PIER 94, 367–382, 2009

ACCURATE AND EFFICIENT EVALUATION OF METHOD OF MOMENTS MATRIX BASED ON A GENERALIZED ANALYTICAL APPROACH

Z. H. Liu

School of Electrical & Electronics Engineering
Nanyang Technological University
50 Nanyang Avenue, Singapore 639798, Singapore

E. K. Chua

Advanced Electronics and Electromagnetics
Institute of High Performance Computing
1 Fusionopolis Way, #16-16 Connexis, Singapore 138632, Singapore

K. Y. See

School of Electrical & Electronics Engineering
Nanyang Technological University
50 Nanyang Avenue, Singapore 639798, Singapore

Abstract—Based on an analytical expression for the integration of the free-space Green's function involving any combination of basis and test functions, an accurate and highly efficient method to determine the Method of Moments matrix has been developed. A full analytical expression is obtained through direct integration of the Taylor's series expansion of the free-space Green's function. Based on the distance between the source and observation points, a criterion is established to reduce the full expression to a much-simplified expression, which speeds up the computational efficiency to fill up the Method of Moments matrix without compromising the solution accuracy.

1. INTRODUCTION

In any method of moments (MoM) formulation, depending on the selection of the basis functions and the test functions, the impedance matrix can be ill-conditioned [1–4]. As such, the overall accuracy

Corresponding author: E. K. Chua (chuaek@ihpc.a-star.edu.sg).

depends very much on accurate evaluation of the integrals, especially diagonal elements of the matrix. Besides accuracy, efficiency is also one of the main concerns. The solution time for MoM consists of the matrix-fill time and the matrix-solve time. The matrix-fill time is the time taken to calculate all the elements of the impedance matrix, whereas, the matrix-solve time is the time taken to solve the matrix. Depending on the matrix size, the matrix-fill time can contribute a significant portion of the total solution time. Many approaches have been reported to reduce the matrix-fill time. One common approach is to employ interpolation method [5–7]. It evaluates impedance matrices at a few selected frequencies and interpolates impedance matrices for the rest of frequencies. The improvement on the overall matrix-fill time depends on the number of simulation frequencies, which can be a several decades. However, the matrix-fill time for a single frequency still takes up substantial amount of time. Another approach is the application of the artificial neural networks (ANN) based model [8, 9]. Its computational efficiency is superior but suffers in solution's accuracy. Subsequently, a hybrid approach that combines neural networks and method of moments (NN-MoM) [10] is proposed to optimize both matrix-fill time and solution accuracy. It employs two trained radial basis function-neural networks (RBF-NN) to calculate majority of elements in the coupling matrix, the rest of elements are calculated using the conventional method. This approach provides better accuracy but does not reduce matrix-fill time significantly. Some researchers use analytical simplification method [11–13] to reduce the impedance equation format from double integral to single integral. This approach effectively reduces the matrix-fill time but it is still not as efficient as the analytical approach for the evaluation of the impedance matrix elements [14–16]. The analytical approach eliminates the need of numerical integration and therefore, reduces the matrix-fill time significantly. Some other fast algorithms can be found in [17–20].

In this paper, an analytical approach is adopted for evaluation of the impedance matrix elements with the objectives of achieving both computational efficiency and solution's accuracy. To obtain analytical expressions for matrix elements, one needs to know the specific basis and test functions. The choice of basis and test functions in the formulation of MoM matrix is very much dependent on the required accuracy and the ease of numerical implementation. The analytical approach proposed in this paper has the flexibility of choosing any combination of basis and test functions, as long as they can be expressed in polynomial form.

For example, in the electric field integral equations (EFIEs)

formulated in Section 2, depending on the choice of basis function and test function, the order of the integrations can range from 2 to 6. If all these integrations are carried out numerically, it will take up a substantial portion of the matrix-fill time. Also, the solution's accuracy depends very much on resolution of the numerical integration. The double integration using analytical expressions has been reported [14, 15]. However, analytical expression for higher order integration has not been reported. Although, third order integration has been provided in [16], the integrations are derived for triangular basis function with line matching only. The major contribution of this paper is to provide the analytical expressions to evaluate higher-order integrals, up to sixth or even higher order, if needed.

2. FORMULATIONS OF ELECTRIC FIELD INTEGRAL EQUATIONS

A typical printed circuit structure will be used as an example for the EFIEs formulation. In most practical applications, the thickness of the conductor (around 0.025 to 0.05 mm) is much smaller than that of substrate (around 0.8 to 1.6 mm). Therefore, the conductor can be approximated as two-dimensional (2D) perfect electric conductor (PEC) (zero thickness). The substrate used in PCB is assumed to be homogeneous, isotropic and lossless with a defined dielectric constant.

Under the influence of an incident electric field $\mathbf{E}^i$, a PCB as shown in Figure 1, causes a scattered electric field $\mathbf{E}^s$. Then, the resultant electric field $\mathbf{E}$ in free-space will be given as:

$$\mathbf{E} = \mathbf{E}^i + \mathbf{E}^s \tag{1}$$

From [21], the scattered fields are given as follows:

$$\mathbf{E}_c^s(\mathbf{r}) = -j\omega\mu_o \iint\limits_{S_c} \mathbf{J}_c(\mathbf{r}')G(\mathbf{r};\mathbf{r}')ds' + \frac{\nabla}{j\omega\varepsilon_o} \iint\limits_{S_c} \nabla'\cdot\mathbf{J}_c(\mathbf{r}')G(\mathbf{r};\mathbf{r}')ds' \tag{2}$$

$$\begin{aligned}\mathbf{E}_d^s(\mathbf{r}) = &-j\omega\mu_o \iiint\limits_{V_d} \mathbf{J}_d(\mathbf{r}')G(\mathbf{r};\mathbf{r}')dv' + \frac{\nabla}{j\omega\varepsilon_o} \iiint\limits_{V_d} \nabla'\cdot\mathbf{J}_d(\mathbf{r}')G(\mathbf{r};\mathbf{r}')dv' \\ &+ \frac{\nabla}{j\omega\varepsilon_o} \iint\limits_{S_c\cap V_d} \mathbf{J}_d\left(\mathbf{r}'\right)_{norm} G\left(\mathbf{r};\mathbf{r}'\right) ds'\end{aligned} \tag{3}$$

where

$\mathbf{r}'$ — position vector of the source point

$\mathbf{E}_c^s(\mathbf{r})$ — scattered electric field due to the conductor

$\mathbf{E}_d^s(\mathbf{r})$ — scattered electric field due to the substrate

$\mathbf{J}_c(\mathbf{r}')$ — 2D conduction current density on the 2D conductor surface

$\mathbf{J}_d(\mathbf{r}')$ — 3D polarization current density within the substrate

$\mathbf{J}_d(\mathbf{r}')_{norm}$ — 3D normal polarization current density at conductor/substrate boundary

$G(\mathbf{r};\mathbf{r}')$ is the free-space Green's function and is given by:

$$G\left(\mathbf{r};\mathbf{r}'\right) = \frac{e^{-jk_o|\mathbf{r}-\mathbf{r}'|}}{4\pi\left|\mathbf{r}-\mathbf{r}'\right|} \tag{4}$$

and the free-space wave number is given as

$$k_o = \omega\sqrt{\mu_o\varepsilon_o} \tag{5}$$

By choosing the basis functions of $\mathbf{J}_c(\mathbf{r}')$, $\mathbf{J}_d(\mathbf{r}')$ and $\mathbf{J}_d(\mathbf{r}')_{norm}$ to be $\boldsymbol{\beta}_c(\mathbf{r}')$, $\boldsymbol{\beta}_d(\mathbf{r}')$ and $\boldsymbol{\beta}_b(\mathbf{r}')$, respectively, and left out all the coefficients and constants, only two types of integral $\mathbf{g}_1(\mathbf{r};\mathbf{r}')$ and $\mathbf{g}_2(\mathbf{r};\mathbf{r}')$ are required.

$$\mathbf{g}_1\left(\mathbf{r};\mathbf{r}'\right) = \int_{\beta_j} \boldsymbol{\beta}_j\left(\mathbf{r}'\right) G\left(\mathbf{r};\mathbf{r}'\right) d\beta_j \tag{6}$$

$$\mathbf{g}_2\left(\mathbf{r};\mathbf{r}'\right) = \nabla \int_{\beta_j} \nabla' \cdot \boldsymbol{\beta}_j\left(\mathbf{r}'\right) G\left(\mathbf{r};\mathbf{r}'\right) d\beta_j \tag{7}$$

where $j = c,\ d$ or b and $\boldsymbol{\beta}_j$ is the region of integration of the basis function $\boldsymbol{\beta}_j(\mathbf{r}')$. By choosing $\theta_i(\mathbf{r})$ to be the test function and applying the MoM procedure, (6) and (7) become (8) and (9), respectively:

$$Z_1\left(\mathbf{r};\mathbf{r}'\right) = \int_{\theta_i} \theta\left(\mathbf{r}\right) \int_{\beta_j} \boldsymbol{\beta}_j\left(\mathbf{r}'\right) G\left(\mathbf{r};\mathbf{r}'\right) d\beta_j d\theta_i \tag{8}$$

$$Z_2\left(\mathbf{r};\mathbf{r}'\right) = \int_{\theta_i} \theta\left(\mathbf{r}\right) \nabla \int_{\beta_j} \nabla' \cdot \boldsymbol{\beta}_j\left(\mathbf{r}'\right) G\left(\mathbf{r};\mathbf{r}'\right) d\beta_j d\theta_i \tag{9}$$

where $i = c$, d or b and θ_i is the region of integration of the test function $\theta_i(\mathbf{r})$.

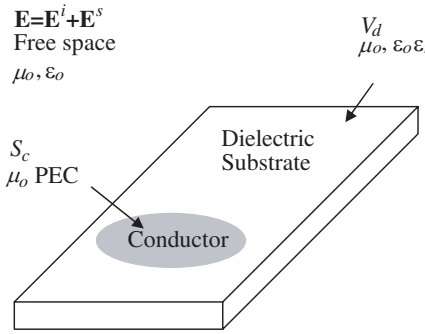

Figure 1. Finite-size printed circuit structure.

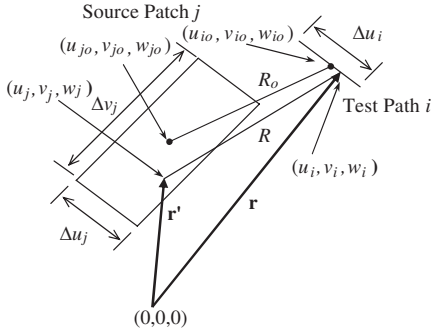

Figure 2. Source region and test interval.

3. EXPANSION OF FREE-SPACE GREEN'S FUNCTION

In the past, direct integration of $G(\mathbf{r};\mathbf{r}')$ is not readily available until Alatan, et al., expanded $G(\mathbf{r};\mathbf{r}')$ in Taylor's series around R_o [15].

$$\frac{e^{-jk_oR}}{4\pi R} \approx \frac{e^{-jk_oR_o}}{4\pi R}\sum_{p=0}^{n}\frac{(-j)^p\,k_o^p\,(R-R_o)^p}{p!} \tag{10}$$

where $R = |\mathbf{r}-\mathbf{r}'|$. As long as $|R-R_o|$ is sufficiently small, $G(\mathbf{r};\mathbf{r}')$ can be approximated by only a few terms of Taylor's series expansion. The error bound of the series depends on the number of terms to be included in calculation. The error bound of (10) up to nth order can be obtained by

$$\text{error} \le \left|\frac{e^{-jk_oR_o}}{4\pi R}\right|\left|\frac{k_o^{n+1}(R-R_o)^{n+1}}{(n+1)!}\right| + O\left(R^{n+2}\right) \tag{11}$$

Once $G(\mathbf{r};\mathbf{r}')$ is expanded in Taylor's series, analytical expressions for the integration of $G(\mathbf{r};\mathbf{r}')$ can be derived. To determine error bound of the series, Figure 2 is an example used to illustrate the procedure.

Figure 2 shows an example of a source patch where the basis function is situated and an observation line path (line matching test function); $\mathbf{r}'$ and $\mathbf{r}$ are the position vectors for the source and observation points, respectively. The distance between the observation point (u_i, v_i, w_i) and source point (u_j, v_j, w_j) is R. The distance between midpoint of the line path (u_{io}, v_{io}, w_{io}) and the centre of the source patch (u_{jo}, v_{jo}, w_{jo}) is R_o. It can be observed from Figure 2 that the maximum distance between R and R_o occurs when both (u_{io}, v_{io}, w_{io}) and (u_{jo}, v_{jo}, w_{jo}) lie on the same point. This distance

Table 1. Error bound of $\max|R - R_o|$.

Basis function/Test function	$\max\|R - R_o\|$
point/point (0D/0D)	0
line/point (1D/0D)	0.05λ
surface/point (2D/0D)	$0.05\sqrt{2}\lambda$
volume/point (3D/0D)	$0.05\sqrt{3}\lambda$
line/line (1D/1D)	0.1λ
surface/line (2D/1D)	$0.05\sqrt{5}\lambda$
volume/line (3D/1D)	$0.05\sqrt{6}\lambda$
surface/surface (2D/2D)	$0.1\sqrt{2}\lambda$
volume/surface (3D/2D)	0.15λ
volume/volume (3D/3D)	$0.1\sqrt{3}\lambda$

can be calculated by:

$$\max|R - R_o| = \sqrt{(\Delta u_j)^2 + (\Delta v_j/2)^2} = 0.05\sqrt{5}\lambda \tag{12}$$

where $\Delta u_i = \Delta u_j = \Delta v_j = 0.1\lambda$ and λ is the wavelength. Many different combinations of basis and test functions were available. Table 1 shows the error bound of $\max|R - R_o|$ for the typical combinations of basis and test functions.

By assuming the maximum grid size for the structure in the modeling to be 0.1λ, Table 2 shows the error bound of (10) for one-dimension basis function/one-dimension test function (1D/1D), two-dimension basis function/two-dimension test function (2D/2D) and three-dimension basis function/three-dimension test function (3D/3D) with various order, n.

From Table 2, the worst error bound of (10) for 3D/3D case up to 5th order is 0.231%. It is sufficiently accurate for most engineering problems. However if accuracy of better than 0.1% error bound is required, (10) will be truncated till higher order terms. By applying the binomial expansion to $(R - R_o)^p$, (10) can be rewrite as (13).

$$\frac{e^{-jk_oR}}{4\pi R} \approx \frac{e^{-jk_oR_o}}{4\pi R} \sum_{p=0}^{n} \beta_p R^p \tag{13}$$

where

$$\beta_p = \sum_{m=p}^{n} (-1)^{2m-p} \frac{(j)^m k_o^m}{p!\,(m-p)!} R_o^{m-p} \tag{14}$$

Table 2. Error bound of (10).

Order n	1D/1D	2D/2D	3D/3D
0	62.8%	88.9%	109%
1	19.7%	19.7%	59.2%
2	4.13%	11.7%	21.5%
3	0.649%	2.60%	5.84%
4	0.0816%	0.462%	1.27%
5	0.00855%	0.0684%	0.231%
6	0.000767%	0.00868%	0.0359%

With (13), analytical expression for the integration of $G(\mathbf{r};\mathbf{r}')$ is now possible since all the terms in (13) have closed form integrals.

4. ANALYTICAL EXPRESSIONS FOR INTEGRALS

As long as both the basis and test functions are in polynomial forms, only one kind of integration is required to solve, which is given in (15),

$$g\left(u,v,w\right) = \int\limits_{\Omega_T} u^m f\left(u,v,w\right) d\Omega_T \tag{15}$$

where Ω_T is the integration domain (the domain can be line (1D), area (2D) or volume (3D)) for test function and

$$f\left(u,v,w\right) = \int\limits_{\Omega_B} u^m R^n d\Omega_B \tag{16}$$

where $R = \sqrt{u^2+v^2+w^2}$ and Ω_B is the integration domain for basis function. Similarly, the domain can be line (1D), area (2D) or volume (3D). Since analytical expressions for the integrations of even-powered R terms are easily obtainable, only the integrations of odd-powered terms are discussed from this point onwards. The full expressions of (16) can be obtained from Appendix A and then the full expression of (15) can be evaluated by making full use of the solutions of the integrals given in Appendix A. For simplicity, only the expressions for single, double and triple integrals are given Appendix A. Higher order integrals can be evaluated by further integrating the triple integrals. Appendix A has given all the necessary integral expressions. From

detail study, only the six integrals listed as follow are required to evaluate (15) and (16).

$$\int u^m R^n du \qquad \int u^n \left(u^2+w^2\right)^{-1} R^{-1} du$$

$$\int u^n \tanh^{-1}\left(uR^{-1}\right) du \qquad \int u^n \tanh^{-1}\left(vR^{-1}\right) du$$

$$\int u^n \tan^{-1}\left(vwu^{-1}R^{-1}\right) du \qquad \int u^n \tan^{-1}\left(uwv^{-1}R^{-1}\right) du$$

A close observation reveals that the integral expressions of (15) and (16) consist of arctangent and logarithmic functions (full expressions are given in Appendix A). From the computational efficiency perspective, these functions should be avoided as much as possible, as they are subroutines in the computer program which require time to compute. As matrix size increases, the total time taken to compute all the matrix elements involving these functions can be substantial. To avoid the use of these functions, all odd-powered R terms (example $1/R$, R and R^3) in (13) are further expanded in terms of Taylor's series around R_o.

$$a_\alpha\left(u',v',w'\right) = R^\alpha \approx \sum_{m=0}^{N}\sum_{n=0}^{N-m}\sum_{p=0}^{N-m-n} A_{\alpha,mnp} u'^m v'^n w'^p \qquad (17)$$

where N is the number of order truncated in the Taylor's series expansion, $R=\sqrt{\left(u_o+u'\right)^2+\left(v_o+v'\right)^2+\left(w_o+w'\right)^2}$ and α is integer.

The coefficient $A_{\alpha,mnp}$ is defined as follows:

$$A_{\alpha,mnp} = \frac{a_\alpha^{(m,n,p)}\left(u_o,v_o,w_o\right)}{m!n!p!}$$

where

$$a_\alpha^{(m,n,p)}\left(u_o,v_o,w_o\right) \equiv \frac{\partial^m\partial^n\partial^p}{\partial u'^m\partial v'^n\partial w'^p} a_\alpha\left(u_o,v_o,w_o\right)$$

To have a clear picture on how the expression looks like, an example for $\alpha=-1$ is given as follow:

$$\begin{aligned} a_{-1}\left(u',v',w'\right) &= \frac{1}{R} \approx \sum_{m=0}^{N}\sum_{n=0}^{N-m}\sum_{p=0}^{N-m-n} A_{-1,mnp} u'^m v'^n w'^p \\ &= \frac{1}{R_o} - \frac{u_o}{R_o^3}u' - \frac{v_o}{R_o^3}v' - \frac{w_o}{R_o^3}w' + \frac{3u_o v_o}{R_o^5}u'v' \end{aligned}$$

$$+\frac{3u_o w_o}{R_o^5}u'w' + \frac{3v_o w_o}{R_o^5}v'w' - \frac{15u_o v_o w_o}{R_o^7}u'v'w' + , \ldots ,$$

With (17), all odd-powered R terms can now be easily integrated by using simple mathematical operation without involving the arctangent and logarithmic subroutines.

The only drawback of (17) is that it cannot be used when the distance between observation point and source point is approaching zero due to the singularity natures of (17). Through experiment, it is found that large error occurs when $R_o < \max(\Delta u_j, \Delta v_j, \Delta w_j)$ and the error is nearly negligible when $R_o \geq 2\max(\Delta u_j, \Delta v_j, \Delta w_j) + \Delta u_i$. Hence, the use of Taylor's series expansions in (17) is restricted to $R_o \geq 2\max(\Delta u_j, \Delta v_j, \Delta w_j) + \Delta u_i$. The limits of the two regions are defined in Table 3. For Region I, the integrals will have to be carried out with the usual arctangent and logarithmic functions. However, most of the matrix elements have satisfied the criterion of Region II except the diagonal and near-diagonal matrix elements. For example if $\Delta u_i = \Delta u_j = \Delta v_j$, only the self-element, the adjacent elements and elements next to the adjacent elements (total nine elements) fall in Region I, the rest of the elements fall in Region II.

5. EFFICIENCY AND ACCURACY OF ANALYTICAL METHOD TO COMPUTE THE MOM MATRIX

To demonstrate the computational efficiency of the proposed analytical method, triangular basis function with line matching test function is selected to solve the EFIEs described in (2)–(3) with the number of term n in (13) used for Taylor's series expansion is set to 5 and the number of term N in (17) is set to 5 as well. By applying the MoM procedure, only four different kinds of integration are required to solve. These are surface integration of 2D pulse function ($I_{2D\Pi}$), volume integration of 3D pulse function ($I_{3D\Pi}$), triple integration of 2D triangular function ($I_{2D\Lambda}$) and quadruple integration of 3D triangular function ($I_{3D\Lambda}$). Their mathematical expressions are given by:

$$I_{2\mathrm{D}\Pi} = \frac{1}{4\pi}\int_{-\frac{\Delta v_j}{2}}^{\frac{\Delta v_j}{2}}\int_{-\frac{\Delta u_j}{2}}^{\frac{\Delta u_j}{2}}\frac{e^{-jk_o R}}{R}du_j dv_j \tag{18}$$

Table 3. Region definitions.

Region I	Region II
$R_o < 2\max(\Delta u_i \Delta v_i \Delta w_i) + \Delta u_i$	$R_o \geq 2\max(\Delta u_i \Delta v_i \Delta w_i) + \Delta u_i$

Table 4. CPU times for one matrix element using different methods.

	16-point quadrature	128-point quadrature	Region I	Region II
$I_{2D\Pi}$	0.0422 ms	2.66 ms	0.937 μs	0.422 μs
$I_{2D\Lambda}$	0.6844 ms	349.69 ms	2.734 μs	0.672 μs
$I_{3D\Pi}$	0.6515 ms	333.6 ms	3.032 μs	0.5 μs
$I_{3D\Lambda}$	10.5813 ms	43.575 s	8.61 μs	0.718 μs

$$I_{2D\Lambda} = \frac{1}{4\pi}\int_{-\frac{\Delta u_i}{2}}^{\frac{\Delta u_i}{2}}\int_{-\frac{\Delta v_j}{2}}^{\frac{\Delta v_j}{2}}\int_{-\frac{\Delta u_j}{2}}^{\frac{\Delta u_j}{2}}\frac{e^{-jk_oR}}{R}\left(\frac{1}{2}\pm\frac{u_j}{\Delta u_j}\right)du_jdv_jdu_i \quad (19)$$

$$I_{3D\Pi} = \frac{1}{4\pi}\int_{-\frac{\Delta w_j}{2}}^{\frac{\Delta w_j}{2}}\int_{-\frac{\Delta v_j}{2}}^{\frac{\Delta v_j}{2}}\int_{-\frac{\Delta u_j}{2}}^{\frac{\Delta u_j}{2}}\frac{e^{-jk_oR}}{R}du_jdv_jdw_j \quad (20)$$

$$I_{3D\Lambda} = \frac{1}{4\pi}\int_{-\frac{\Delta u_i}{2}}^{\frac{\Delta u_i}{2}}\int_{-\frac{\Delta w_j}{2}}^{\frac{\Delta w_j}{2}}\int_{-\frac{\Delta v_j}{2}}^{\frac{\Delta v_j}{2}}\int_{-\frac{\Delta u_j}{2}}^{\frac{\Delta u_j}{2}}\frac{e^{-jk_oR}}{R} \times\left(\frac{1}{2}\pm\frac{u_j}{\Delta u_j}\right)du_jdv_jdw_jdu_i \quad (21)$$

Computation times for a matrix element using 16-point quadrature integration, 128-point quadrature integration, analytical expression for Region I (defined in Table 3) and analytical expression for Region II (defined in Table 3 as well) are compared and tabulated in Table 4. All results provided in Table 4 are obtained using a Pentium D 820 CPU (2.8 GHz). Taking the 16-point quadrature integration as the reference, relative speed improvement factors for computing $I_{2D\Pi}$, $I_{2D\Lambda}$, $I_{3D\Pi}$ and $I_{3D\Lambda}$, respectively, are nearly 40, 250, 210, 1200 for Region I and 100, 1000, 1300, 14000 for Region II, respectively.

A microstrip line structure with load end short-circuited, as shown in Figure 3, is used as a test case. The dimensions of the microstrip line: length = 100 mm, width = 1 mm, thickness = 1 mm and ground plane width = 5 mm. The microstrip line structure is subdivided with equal rectangular cells 2.5 mm by 1 mm by 1 mm. The matrix size of the microstrip line structure is 995 by 995. Since, we use equal rectangular cell in this example, many matrix elements have same values and will only need to calculate once. This will greatly reduce the overall matrix-fill time. Table 5 shows that matrix-fill time is reduced by nearly 20 times with respect to the 16-points quadrature approach

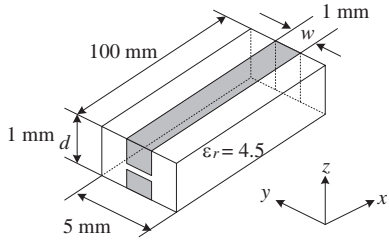

Figure 3. A short-circuited microstrip line.

Table 5. Matrix-fill times for microstrip structure using different methods.

	16-point quadrature	128-point quadrature	Proposed method
Microstrip	14.484 s	53,200.791 s	0.703 s

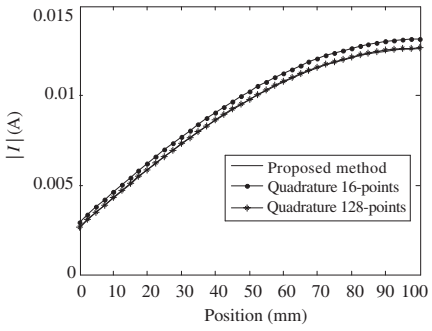

Figure 4. Current distributions of the short-circuited microstrip line at 350 MHz.

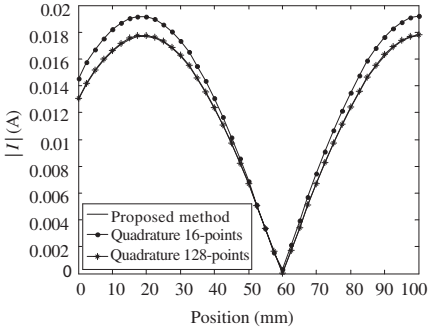

Figure 5. Current distributions of the short-circuited microstrip line at 1 GHz.

or 75,000 times with respect to the 128-points quadrature approach.

To verify the solution accuracy, the current distributions along the short-circuited microstrip line at 350 MHz (the resonant frequency) and 1 GHz with 1 V excitation source, using the analytical method, the 16-point quadrature integration and the 128-point quadrature integration are shown in Figure 4 and Figure 5, respectively.

The comparisons show that the analytical method proposed in the paper is in very good agreement with the 128-point quadrature integration method. The 16-point quadrature integration method produces significantly higher current than the other two methods. The discrepancy is expected because the 16-point quadrature integration is expected to incur larger error in the integration.

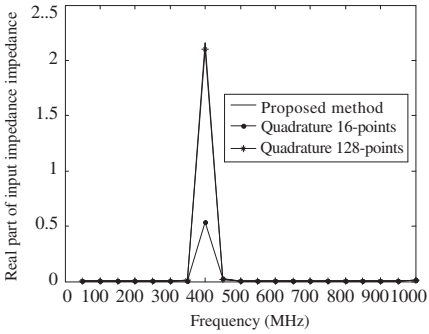

Figure 6. Input impedance of the short-circuited microstrip line (real part).

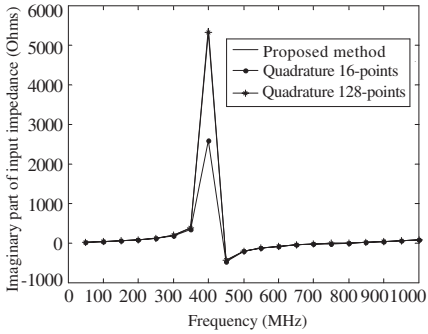

Figure 7. Input impedance of the short-circuited microstrip line (imaginary part).

The plots of real and imaginary parts of input impedance versus frequency of the short-circuited microstrip line using the three approaches are shown in Figure 6 and Figure 7, respectively. Again, the analytical method is in close agreement with the 128-point quadrature integration method. The 16-points quadrature integration method matches quite well with the other two methods but significant discrepancies show up at the resonant frequency.

With the above comparison in both computational speed and accuracy, the analytical method proposed in this paper has been proven to be as accurate as the 128-point quadrature integration method, and also at very much reduced CPU time.

6. CONCLUSION

Through the use of Taylor's series expansion of the free-space Green's function, the analytical expressions for any order of the integration of the Green's function have been developed. Further simplification to these expressions has also been derived by expanding the R terms in terms of Taylor's series. The computational efficiency and accuracy have been discussed, and the proposed method has demonstrated its efficiency and accuracy.

APPENDIX A.

The full expressions of all the integrations required in this paper are listed here. The definition of C_m^n is given by

$$C_m^n = \frac{n!}{m!\,(n-m)!}$$

$$\int R^n du = \begin{cases} u \sum\limits_{p=0}^{(n-1)/2} \left[\dfrac{\prod\limits_{q=0}^{p-1}(n-2q)}{\prod\limits_{q=0}^{p}(n+1-2q)} \left(v^2+w^2\right)^p R^{n-2p} \right] \\ +\left[\prod\limits_{q=0}^{(n-1)/2} \dfrac{(n-2q)}{(n+1-2q)} \right] \left(v^2+w^2\right)^{(n+1)/2} \tanh^{-1}\frac{u}{R}, \\ n = \text{odd} \\ u \sum\limits_{p=0}^{n/2} \left[\dfrac{\prod\limits_{q=0}^{p-1}(n-2q)}{\prod\limits_{q=0}^{p}(n+1-2q)} \left(v^2+w^2\right)^p R^{n-2p} \right], \; n = \text{even} \end{cases}$$

$$\int u^m R^n du = \begin{cases} \sum\limits_{p=0}^{(m-1)/2} (-1)^p C^n_{(m-1)/2} \left(v^2+w^2\right)^p \frac{R^{n+m-2p+1}}{n+m-2p+1}, \\ m = \text{odd} \\ \sum\limits_{p=0}^{m/2} (-1)^p C^n_{m/2} \left(v^2+w^2\right)^p \int R^{n+m-2p} du, \\ m = \text{even} \end{cases}$$

$$\int \frac{u^n}{(u^2+w^2)\,R} du = \begin{cases} \sum\limits_{p=0}^{(n-3)/2} (-1)^p w^{2p} \int \dfrac{u^{n-2-2p}}{R} du \\ +(-1)^{(n-3)/2} v^{-1} w^{n-1} \tanh^{-1}\frac{v}{R}, \quad n = \text{odd} \\ \sum\limits_{p=0}^{n/2-1} (-1)^p w^{2p} \int \dfrac{u^{n-2-2p}}{R} du \\ +(-1)^{n/2} v^{-1} w^{n-1} \tan^{-1}\dfrac{uv}{wR}, \; n = \text{even} \end{cases}$$

$$\int u^n \tanh^{-1}\frac{u}{R} du = \frac{u^{n+1}}{n+1} \tanh^{-1}\frac{u}{R} - \frac{1}{(n+1)} \int \frac{u^{n+1}}{R} du$$

$$\int u^n \tanh^{-1}\frac{v}{R} du = \frac{u^{n+1}}{n+1} \tanh^{-1}\frac{v}{R} + \frac{v}{(n+1)} \int \frac{u^{n+2}}{(u^2+w^2)R} du$$

$$\int u^n \tan^{-1}\frac{vw}{uR} du = \frac{u^{n+1}}{n+1} \tan^{-1}\frac{vw}{uR} + \frac{vw}{(n+1)} \int \frac{u^{n+1}}{(u^2+v^2)\,R} du + \frac{vw}{(n+1)} \int \frac{u^{n+1}}{(u^2+w^2)\,R} du$$

$$\int u^n \tan^{-1}\frac{uw}{vR} du = \frac{u^{n+1}}{n+1} \tan^{-1}\frac{uw}{vR} - \frac{vw}{(n+1)} \int \frac{u^{n+1}}{(u^2+v^2)\,R} du$$

$$\iint R^n dudv = \begin{cases} u\sum\limits_{p=0}^{(n-1)/2}\left[\dfrac{\prod\limits_{q=0}^{p-1}(n-2q)}{\prod\limits_{q=0}^{p}(n+1-2q)}\sum\limits_{s=0}^{p}C_s^p w^s \int v^{p-s}R^{n-2p}dv\right] \\ +\left[\prod\limits_{q=0}^{(n-1)/2}\dfrac{(n-2q)}{(n+1-2q)}\right]\sum\limits_{s=0}^{(n+1)/2}C_s^{(n+1)/2}w^s \\ \times\int v^{(n+1)/2-s}\tanh^{-1}\dfrac{u}{R}dv,\ n=\text{odd} \\ u\sum\limits_{p=0}^{n/2}\left[\dfrac{\prod\limits_{q=0}^{p-1}(n-2q)}{\prod\limits_{q=0}^{p}(n+1-2q)}\sum\limits_{s=0}^{p}C_s^p w^s\int v^{p-s}R^{n-2p}dv\right], \\ n=\text{even} \end{cases}$$

$$\iint u^m R^n dudv = \begin{cases} \sum\limits_{p=0}^{(m-1)/2}(-1)^p C_{(m-1)/2}^n \sum\limits_{s=0}^{p}\dfrac{C_s^p w^s}{n+m-2p+1} \\ \times\int v^{p-s}R^{n+m-2p+1}dv,\ m=\text{odd} \\ \sum\limits_{p=0}^{m/2}(-1)^p C_{m/2}^n\sum\limits_{s=0}^{p}C_s^p w^s \\ \times\int v^{p-s}\int R^{n+m-2p}dudv, m=\text{even} \end{cases}$$

$$\iiint R^n dudvdw = \begin{cases} u\sum\limits_{p=0}^{(n-1)/2}\left[\dfrac{\prod\limits_{q=0}^{p-1}(n-2q)}{\prod\limits_{q=0}^{p}(n+1-2q)}\sum\limits_{s=0}^{p}C_s^p\int w^s\int v^{p-s}R^{n-2p}dvdw\right] \\ +\left[\prod\limits_{q=0}^{(n-1)/2}\dfrac{(n-2q)}{(n+1-2q)}\right]\sum\limits_{s=0}^{(n+1)2}C_s^{(n+1)/2} \\ \times\int w^s\int v^{(n+1)/2-s}\tanh^{-1}\frac{u}{R}dvdw,\ n=\text{odd} \\ u\sum\limits_{p=0}^{n/2}\left[\dfrac{\prod\limits_{q=0}^{p-1}(n-2q)}{\prod\limits_{q=0}^{p}(n+1-2q)}\sum\limits_{s=0}^{p}C_s^p\int w^s\int v^{p-s}R^{n-2p}dvdw\right], \\ n=\text{even} \end{cases}$$

$$\iiint u^m R^n dudvdw = \begin{cases} \sum\limits_{p=0}^{(m-1)/2}(-1)^p C_{(m-1)/2}^n\sum\limits_{s=0}^{p}\dfrac{C_s^p}{n+m-2p+1} \\ \times\int w^s\int v^{p-s}R^{n+m-2p+1}dvdw,\ m=\text{odd} \\ \sum\limits_{p=0}^{m/2}(-1)^p C_{m/2}^n\sum\limits_{s=0}^{p}C_s^p \\ \times\int w^s\int v^{p-s}\int R^{n+m-2p}dudvdw, m=\text{even} \end{cases}$$

REFERENCES

1. Harrington, R. F., *Field Computation by Moment Methods*, 2nd edition, IEEE Press, 1993.
2. Miller, E. K., *Computational Electromagnetics: Frequency-Domain Method of Moments*, IEEE Press, 1992.
3. Peterson, A. F., S. L. Ray, and R. Mittra, *Computational Methods for Electromagnetics*, IEEE Press, 1998.
4. Araujo, M. G., J. M. Bertolo, F. Obelleiro, J. L. Rodriguez, J. M. Taboada, and L. Landesa, "Geometry based preconditioner for radiation problems involving wire and surface basis functions," *Progress In Electromagnetics Research*, PIER 93, 29–40, 2009.
5. Yeo, J. and R. Mittra, "An algorithm for interpolating the frequency variations of method-of-moments matrices arising in the analysis of planar microstrip structures," *IEEE Trans. Microw. Theory & Techn.*, Vol. 51, No. 3, 1018–1025, Mar. 2003.
6. Fasenfest, B. J., F. Capolino, D. R. Wilton, D. R. Jackson, and N. J. Champagne, "A fast MoM solution for large arrays: Green's function interpolation with FFT," *IEEE Antennas and Wireless Propag. Letter*, Vol. 3, No. 9, 161–164, 2004.
7. Soliman, E. A., "Rapid frequency sweep technique for MoM planar solvers," *IEE Proc. Microw. Antennas Propag.*, Vol. 151, No. 4, 277–282, Aug. 2004.
8. Soliman, E. A., A. K. Abdelmageed, and M. A. El-Gamal, "Neural computation of the MoM matrix elements for planar configurations," *Int. J. of Electronics and Communications*, Vol. 56, No. 3, 155–162, 2002.
9. Xiong, Y., D. G. Fang, and Q. J. Zhang, "Application of two-dimensional AWE algorithm in training neural networks," *3rd Int. Conf. on Microw. and Millimeter Wave Tech. Proc.*, 879–882, 2002.
10. Soliman, E. A., H. B. Mohamed, and K. N. Natalia, "Neural networks-method of moments (NN-MoM) for the efficient filling of the coupling matrix," *IEEE Trans. Antennas Propag.*, Vol. 52, No. 6, 1521–1529, Jun. 2004.
11. Tarricone, L., M. Mongiardo, and F. Cervelli, "A quasi one-dimensional integration technique for the analysis of planar microstrip circuits via MPIE/MoM," *IEEE Trans. Microw. Theory & Techn.*, Vol. 49, No. 3, 517–523, Mar. 2001.
12. Smith, J. R. and M. S. Mirotznik, "Analytical simplification of the 2-D method of moments impedance integral," *IEEE Trans. Antennas Propag.*, Vol. 52, No. 12, 3288–3294, Dec. 2004.

13. Smith, J. R. and M. S. Mirotznik, "Moments via integral transform method for 2-D dielectric materials," *IEEE Trans. Antennas Propag.*, Vol. 53, No. 1, 560–563, Jan. 2005.
14. Mahadevan, K. and H. A. Auda, "Electromagnetic field of a rectangular patch of uniform and linear distributions of current," *IEEE Trans. Antennas Propag.*, Vol. 37, No. 12, 1503–1509, Dec. 1989.
15. Alatan, L., M. I. Aksun, K. Mahadevan, and M. T. Birand, "Analytical evaluation of the MoM matrix elements," *IEEE Trans. Microw. Theory & Techn.*, Vol. 44, No. 4, 519–525, Apr. 1996.
16. Chua, E. K., K. Y. See, and Z. H. Liu, "Accurate and efficient computation of MoM matrix involving 2D triangular basis function with line matching," *Int. J. of Computational Methods*, Vol. 3, No. 3, 355–370, Sep. 2006.
17. Wei, X.-C., E. P. Li, and Y. J. Zhang, "Application of the improved finite element-fast multipole method on large scattering problems," *Progress In Electromagnetics Research*, PIER 47, 49–60, 2004.
18. Zhao, P. and H.-G. Wang, "Resistances and inductances extraction using surface integral equation with the acceleration of multilevel green function interpolation method," *Progress In Electromagnetics Research*, PIER 83, 43–54, 2008.
19. Wei, X. C., E. P. Li, and C. H. Liang, "Fast solution for large scale electromagnetic scattering problems using wavelet transform and its precondition," *Journal of Electromagnetic Waves and Applications*, Vol. 17, No. 4, 611–613, 2003.
20. Hussein, K. F. A., "Fast computational algorithm for EFIE applied to arbitrarily-shaped conducting surfaces," *Progress In Electromagnetics Research*, PIER 68, 339–357, 2007.
21. See, K. Y. and E. M. Freeman, "Rigorous approach to modeling electromagnetic radiation from finite-size printed circuit structures," *IEE Proc. Microw., Antenna & Propag.*, Vol. 146, No. 1, 29–34, Feb. 1999.
22. Wei, X. C., E. P. Li, Y. L. Guan, and Y. H. Chong, "Simulation and experimental comparison of different coupling mechanisms for the wireless electricity transfer," *Journal of Electromagnetic Waves and Applications*, Vol. 23, No. 7, 925–934, 2009.